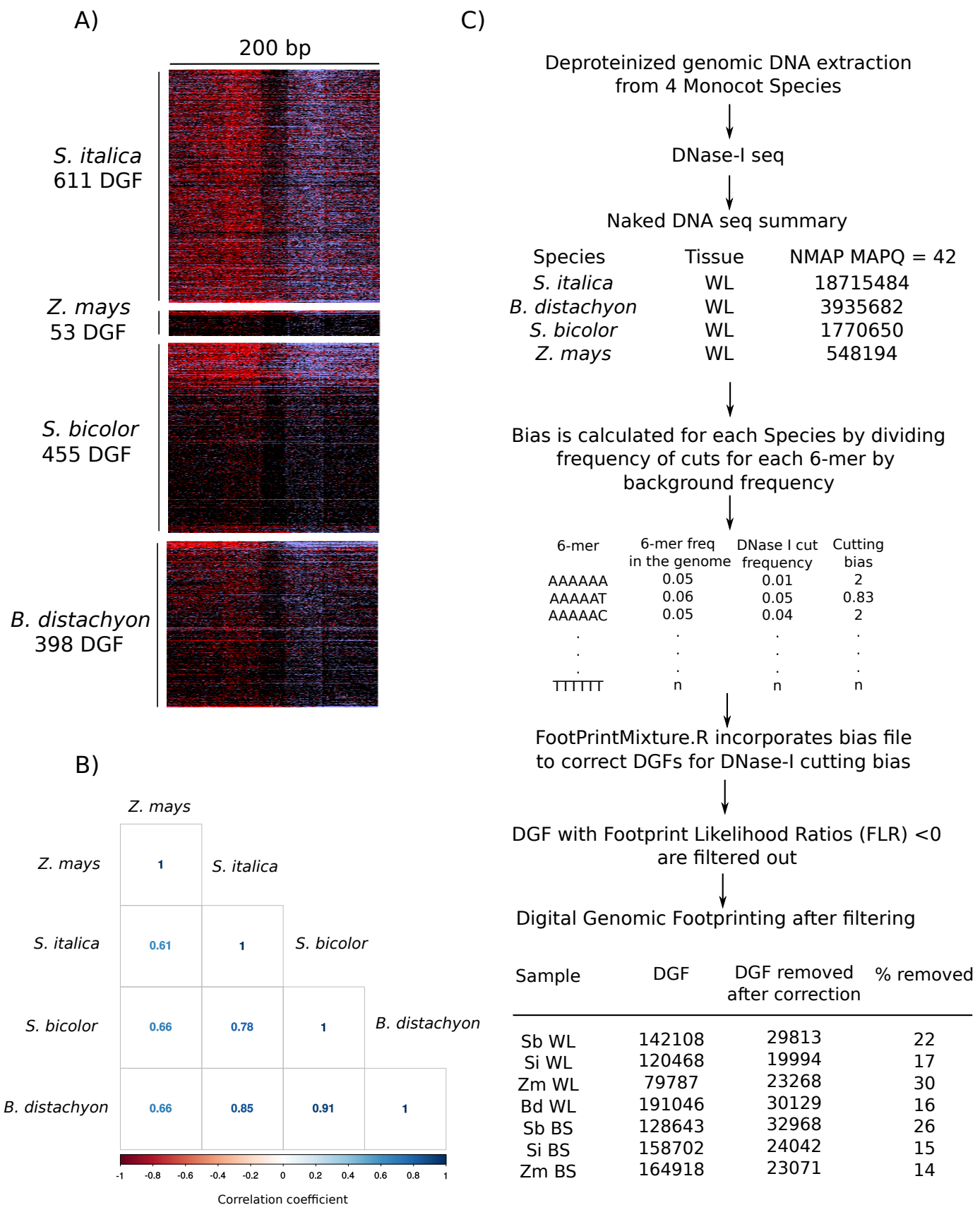


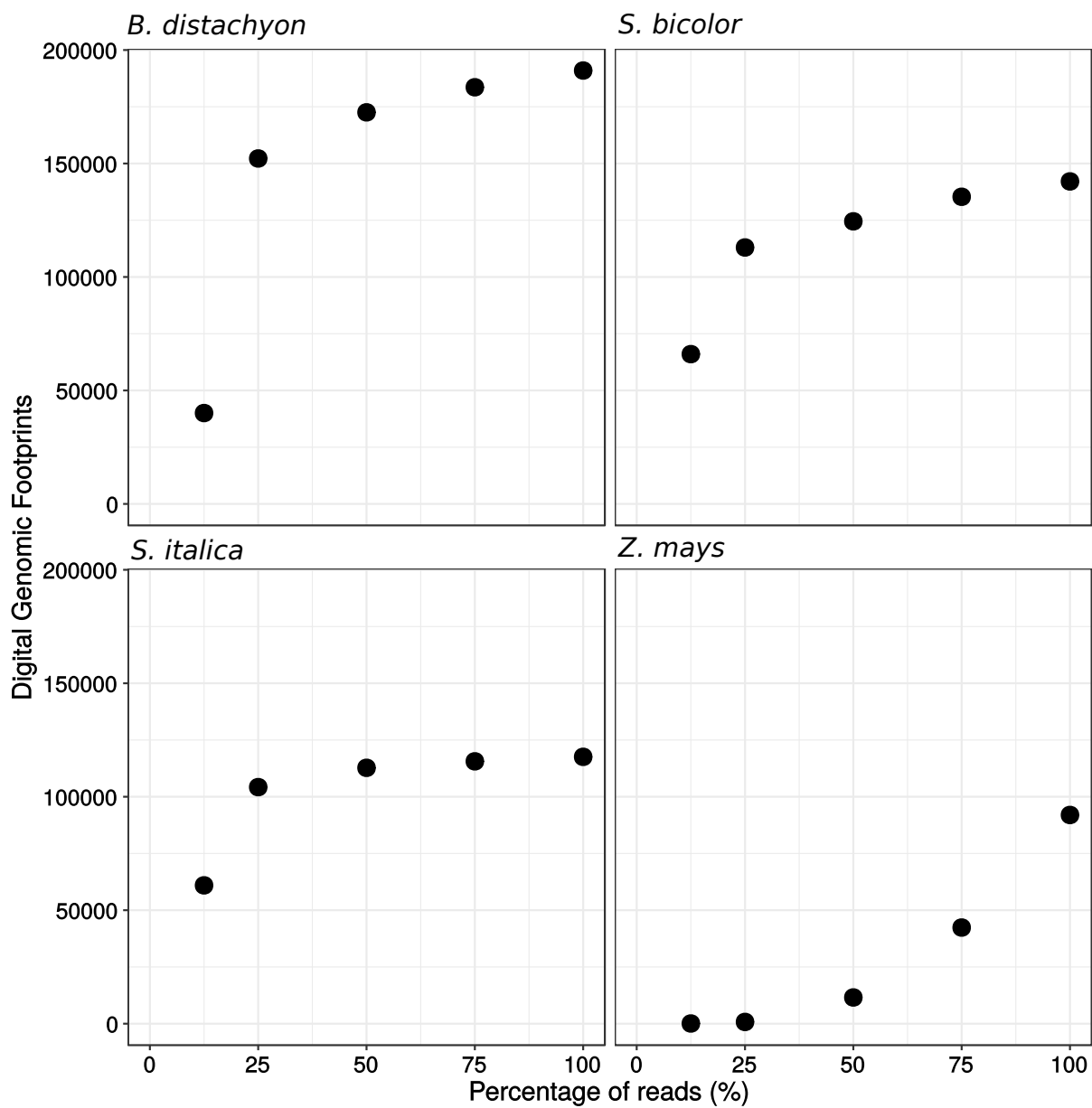
Supplemental Figure 1

**Supplemental Figure 1:** DNasel digestion of nuclei for sequencing. Representative images of digested samples separated on 2% (w/v) agarose gels by electrophoresis. (Supports Figure 1.) (A) *S. bicolor* whole leaf (WL); (B) *S. bicolor* bundle sheath (BS); (C) *Z. mays* WL; (D) *Z. mays* BS; (E) *B. distachyon* WL; (F) *S. italica* WL; (G) *S. italica* BS. Each gel represents a separate biological replicate, and the units of DNasel used are illustrated above. Samples selected for sequencing are indicated in red.



Supplemental Figure 2

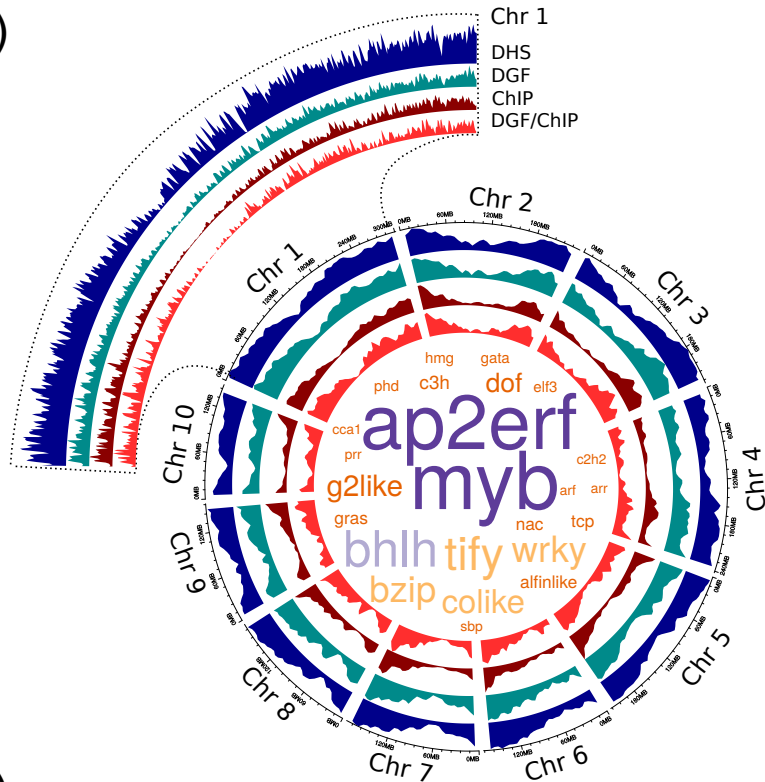
**Supplemental Figure 2:** Bias in DNasel-SEQ cleavage. (Supports Figure 1.) (A) TreeView diagrams illustrating cut density around individual digital genomic footprint (DGFs) predicted from performing DNasel-SEQ on deproteinated genomic DNA from each species. Each row represents an individual DGFs, cuts are coloured according to whether they align to the positive (red) or negative (blue) strand and indicate increased cutting in a 100 bp window on either side of the DGF. (B) Pearson correlation coefficient of DNase I cleavage bias between *Z. mays*, *S. bicolor*, *S. italica* and *B. distachyon*. (C) Schematic illustrating the process adopted to determine DNasel cutting bias and then normalize to allow digital genomic footprinting.



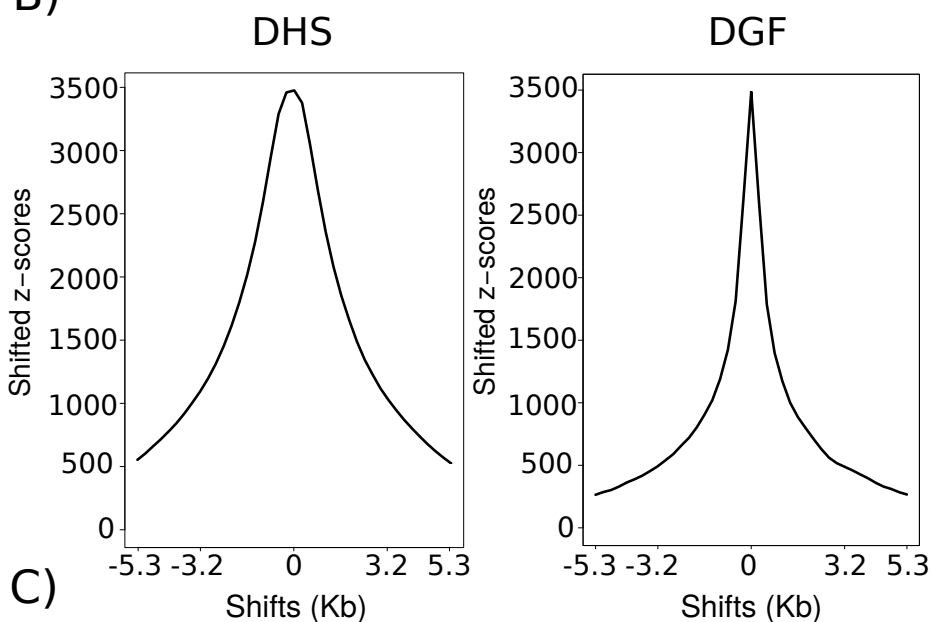
Supplemental Figure 3

**Supplemental Figure 3:** Saturation analysis of footprints. (Supports Figure 1.) Digital genomic footprints were predicted from subsets (12.5, 25, 50, 75 and 100%) of uniquely mapped reads obtained from DNasel-SEQ of whole-leaf samples in each species.

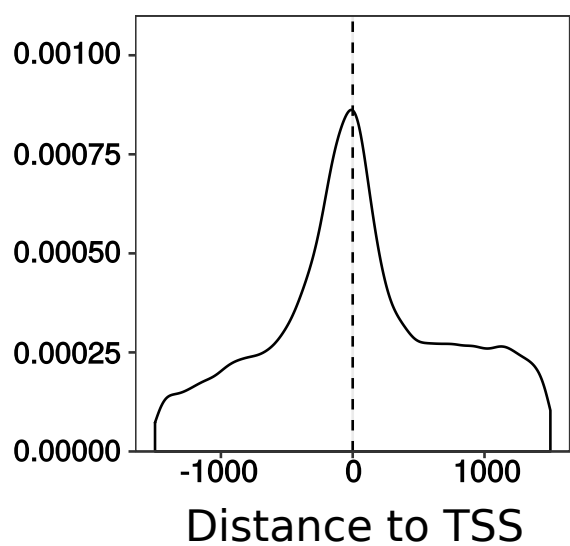
A)



B)

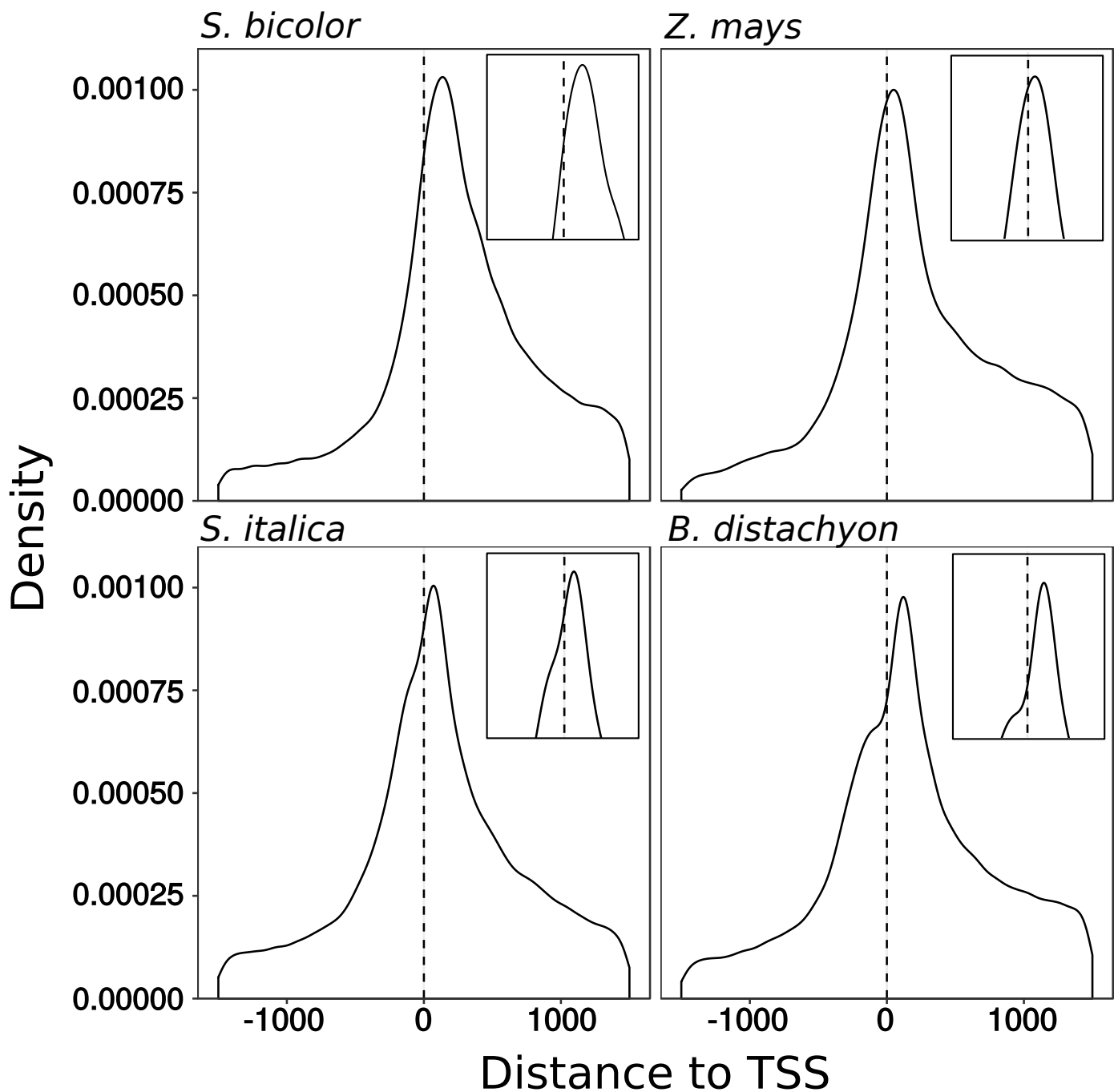


C)



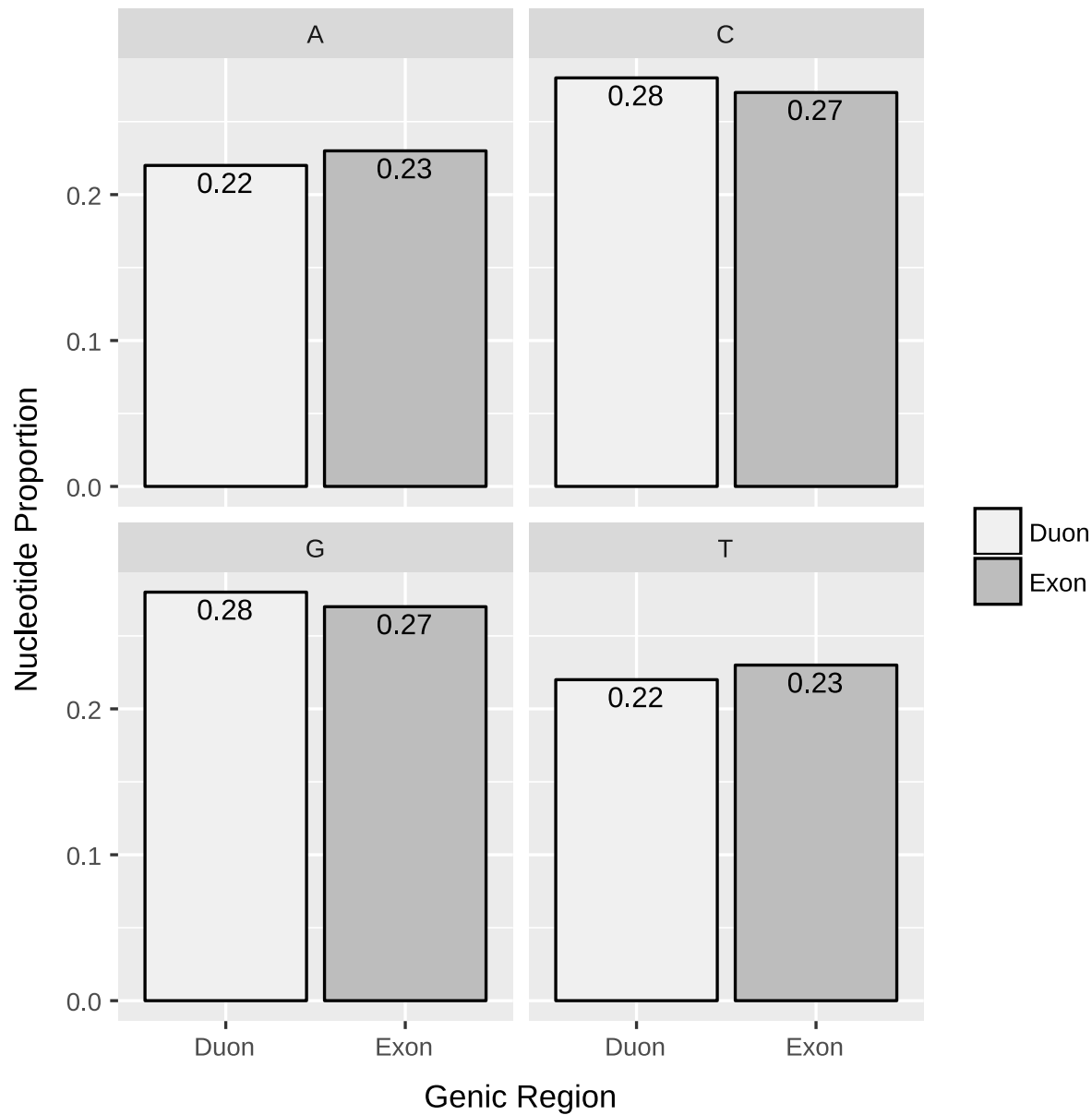
Supplemental Figure 4

**Supplemental Figure 4:** Genome-wide comparison of DGF and ChIP-SEQ peaks from 117 maize transcription factors. (Supports Figure 1 and 2.) (A) Density plot of DHS, DGF, ChIP-SEQ peaks and intersecting DGF/ChIP-SEQ peaks across the maize genome. The center of the plot shows a word cloud representing transcription factor families in the ChIP-SEQ dataset. (B) Effect of shifting DHS and DGF features from their original position on local z-scores as determined by permutation tests between ChIP-SEQ peaks derived from 117 transcription factors. A total of 100 permutations were performed for each comparison. The sharper peak derived from shifting the DGF indicates a higher sensitivity to position and therefore strong overlap with ChIP-SEQ data. (C) Density plot depicting the distribution of ChIP-SEQ signals per kilobase (kb) from the transcription start site (TSS) of *Z. mays*.



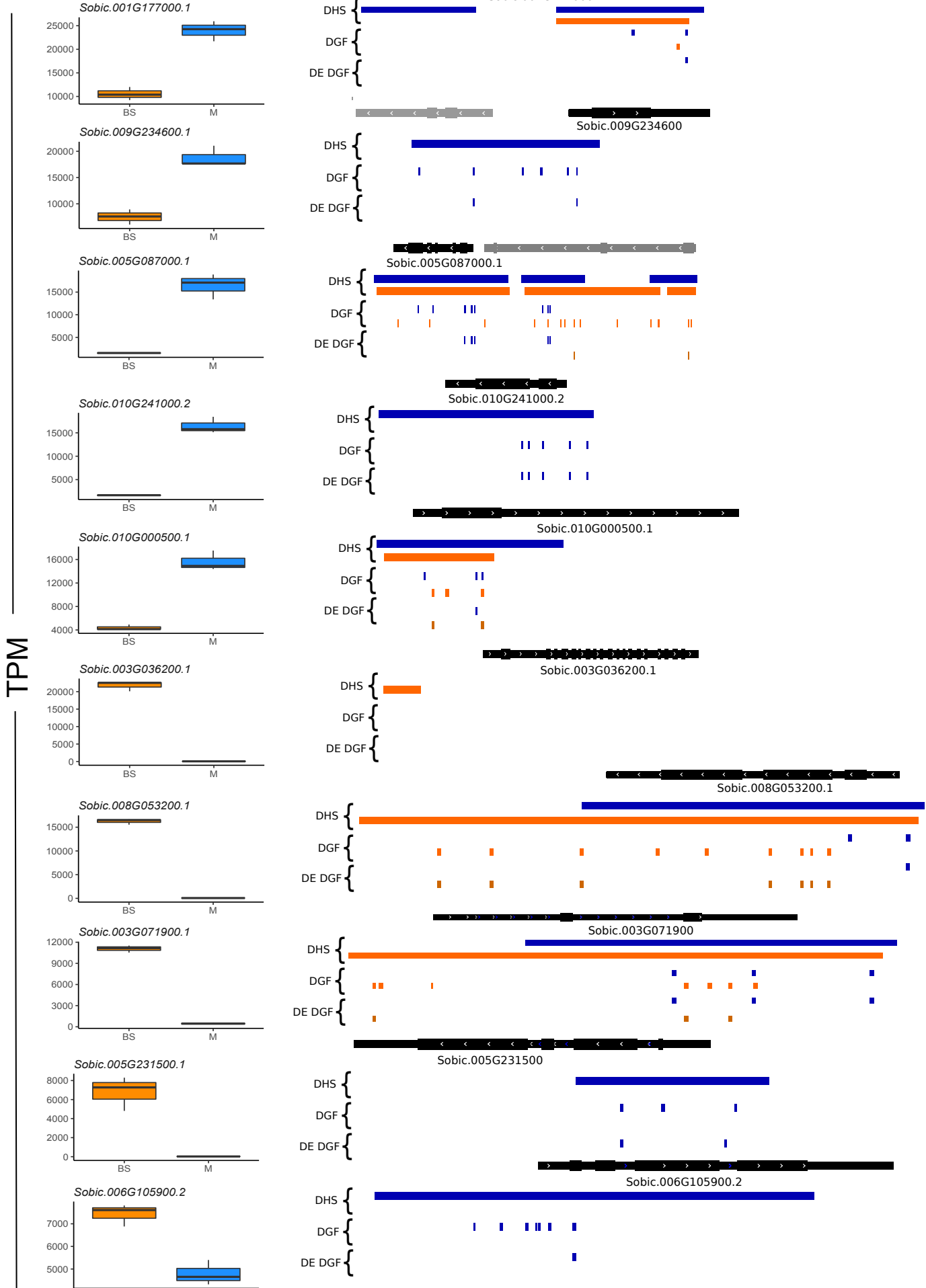
Supplemental Figure 5

**Supplemental Figure 5:** Density plot depicting the distribution of DGFs per kilobase (kb) from the transcription start site (TSS) of *S. bicolor*, *Z. mays*, *S. italica* and *B. distachyon* whole leaves. (Supports Figure 1 & 2.)



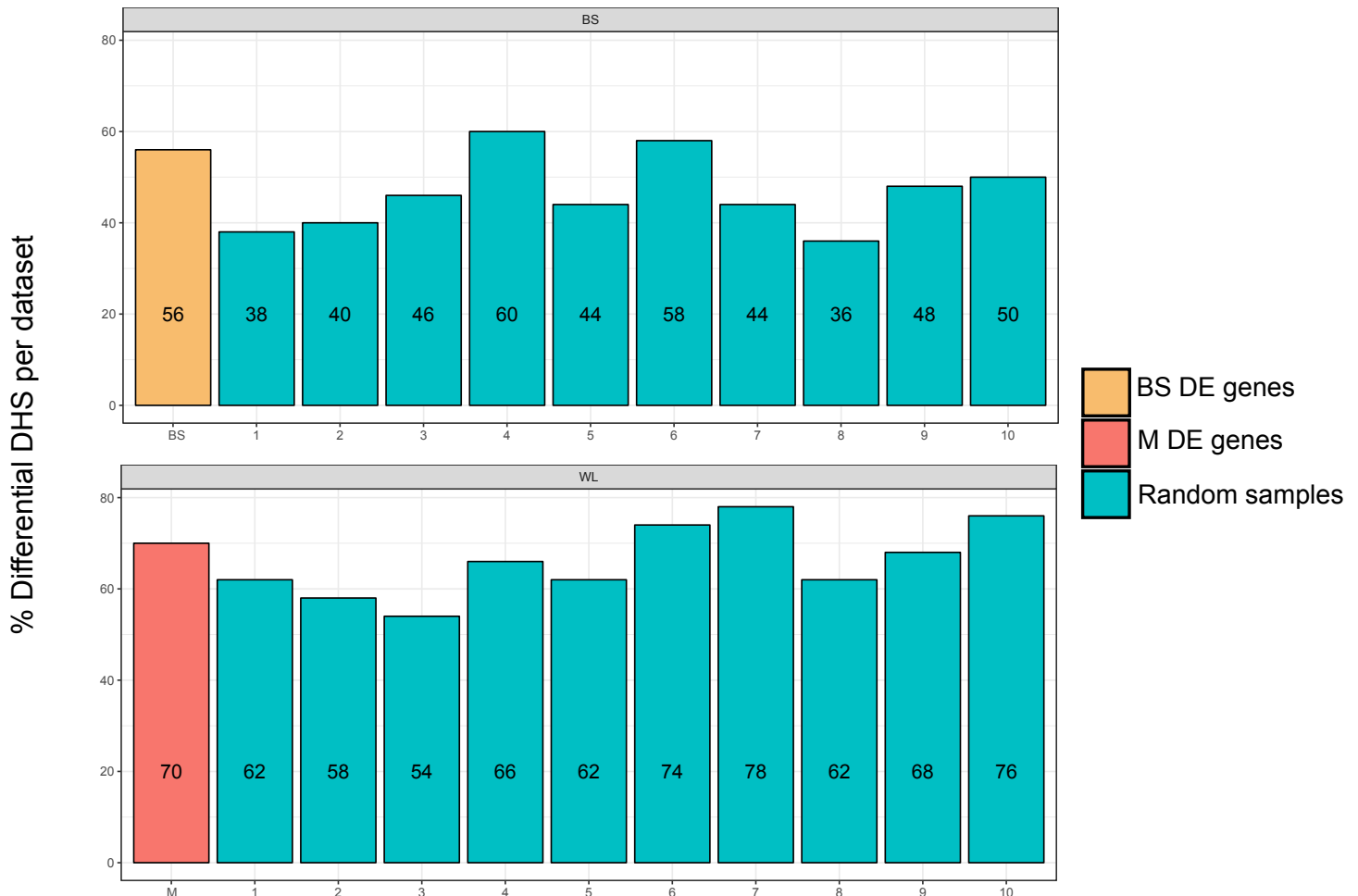
Supplemental Figure 6

**Supplemental Figure 6:** Nucleotide proportion of duons and surrounding exons used in the substitution analysis for *Z. mays*. (Supports Figure 2.) The frequency of each nucleotide was divided by the total length to determine nucleotide proportions across duons as well as surrounding exon sequences.



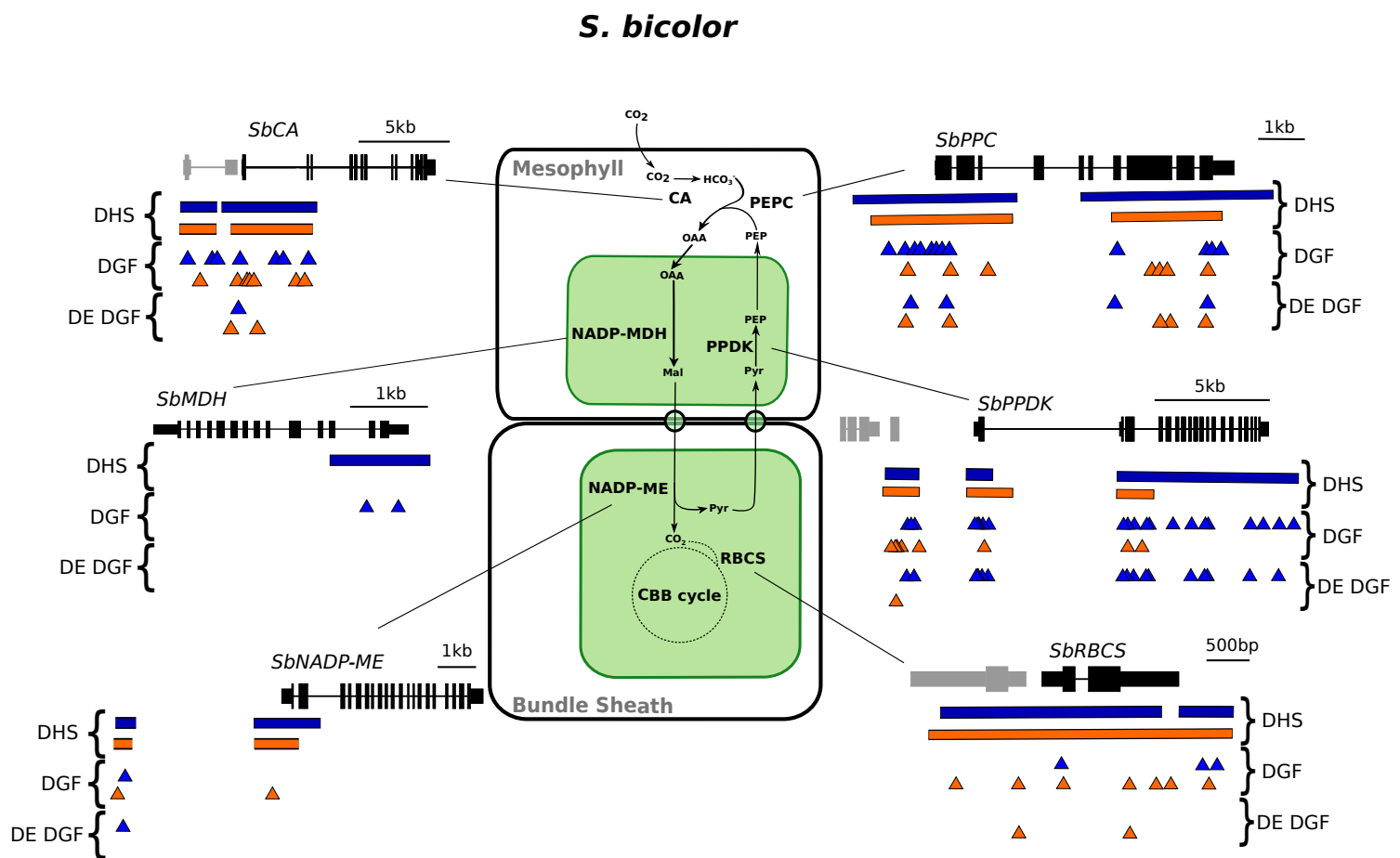
Supplementary Figure 7

**Supplemental Figure 7:** Transcript abundance for genes in mesophyll and bundle-sheath cells associated with DHSs and DGFs in *S. bicolor*. (Supports Figure 3.) (A) Cell preferential gene expression profiles of highly abundant M and BS genes expressed as transcripts per million reads (TPM). (B) Schematic representing DHSs, DGFs and DE DGFs present in whole leaf (blue) and BS (orange) of *S. bicolor*.



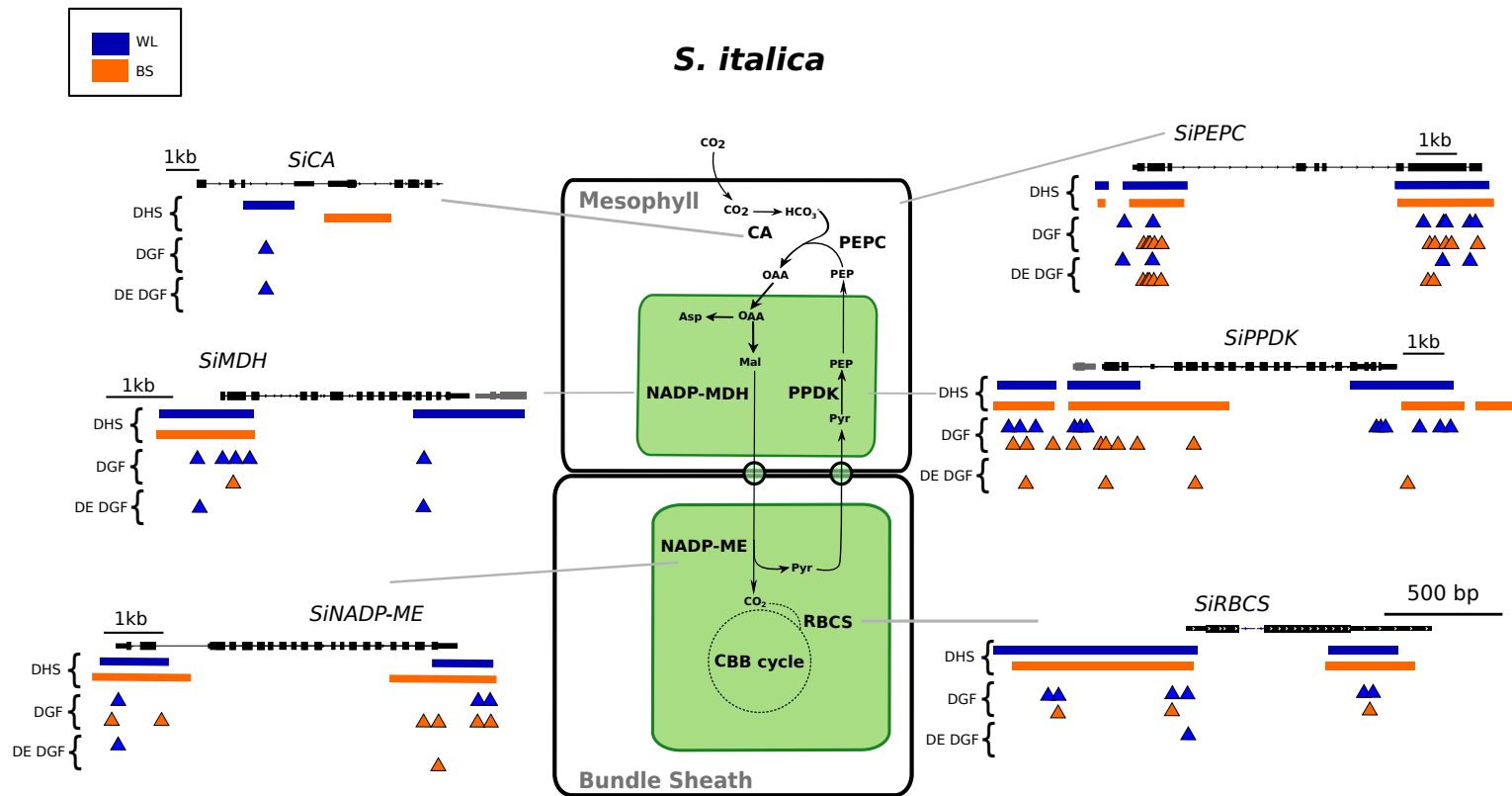
Supplementary Figure 8

**Supplemental Figure 8:** Differential accessibility of broad regulatory regions in *S. bicolor* is not sufficient for cell preferential gene expression. (Supports Figure 3.) Percentage of differentially detected DHSs among BS and M specific genes in *S. bicolor* compared with randomly generated gene samples (n=50).



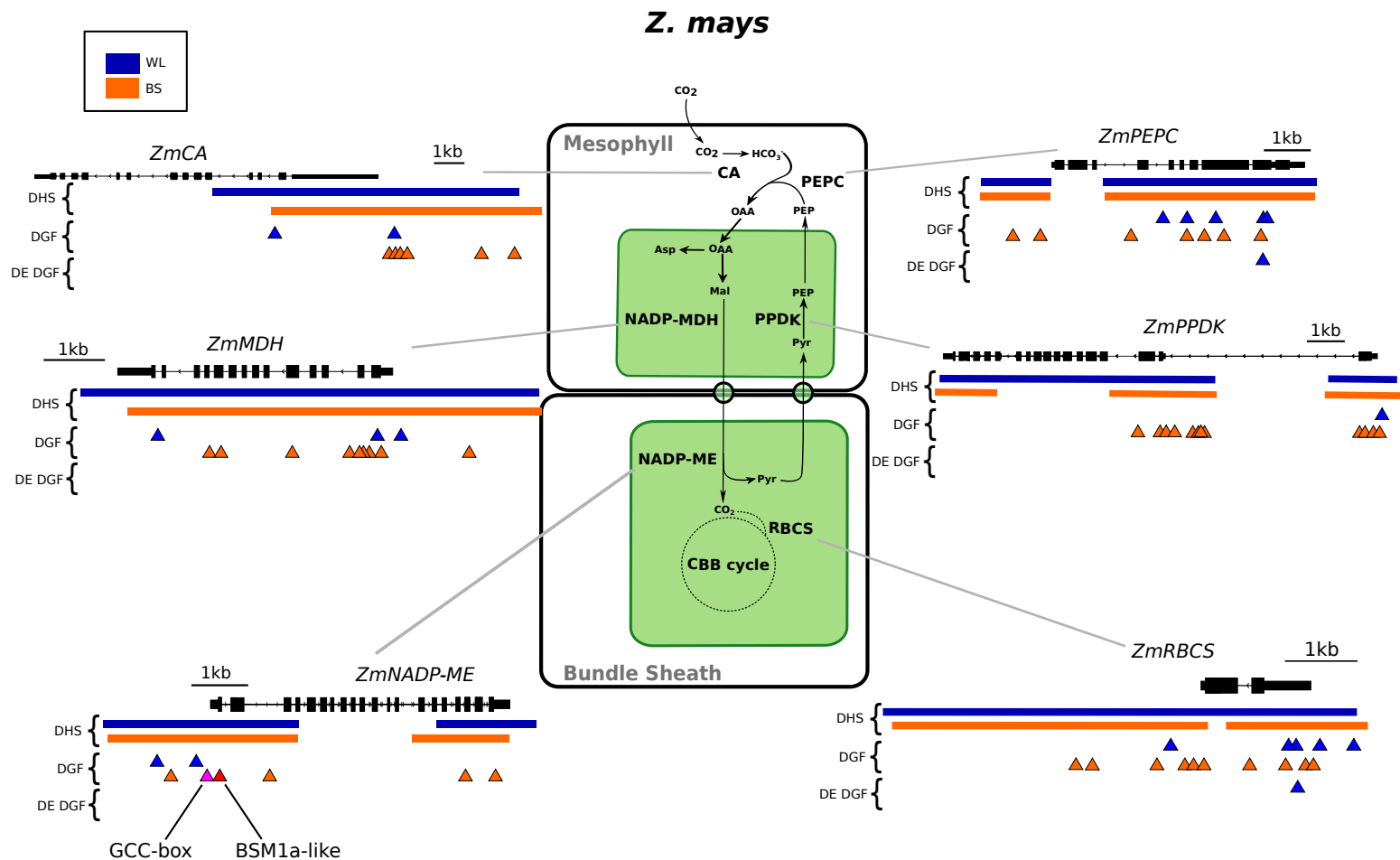
Supplemental Figure 9

**Supplemental Figure 9:** Representation of the C<sub>4</sub> pathway showing differentially accessible DHSs, DGFs and cell-specific DGFs between whole-leaf (blue) and bundle-sheath (orange) samples in *S. bicolor*. (Supports Figure 3.) CA; *Carbonic Anhydrase*, PEPC; *Phosphoenolpyruvate carboxylase*, PPDK; Pyruvate, *orthophosphate dikinase*, MDH; *Malate dehydrogenase*, NADP-ME; *NADP-dependent malic enzyme*, RBCS1A; *Ribulose bisphosphate carboxylase small subunit1A*, OAA; Oxaloacetate, Mal; Malate, PEP; Phosphoenolpyruvate, Pyr; Pyruvate, Asp; Aspartate.



Supplementary Figure 10

**Supplemental Figure 10:** Representation of the C<sub>4</sub> pathway showing differentially accessible DHSs, DGFs and cell-specific DGFs between whole-leaf (blue) and bundle-sheath (orange) samples in *S. italica*. (Supports Figure 3.) CA; *Carbonic Anhydrase*, PEPC; *Phosphoenolpyruvate carboxylase*, PPDK; Pyruvate, *orthophosphate dikinase*, MDH; *Malate dehydrogenase*, NADP-ME; *NADP-dependent malic enzyme*, RBCS1A; *Ribulose bisphosphate carboxylase small subunit1A*, OAA; Oxaloacetate, Mal; Malate, PEP; Phosphoenolpyruvate, Pyr; Pyruvate, Asp; Aspartate.



Supplemental Figure 11

**Supplemental Figure 11:** Representation of the C<sub>4</sub> pathway showing differentially accessible DHSs, DGFs and cell-specific DGFs between whole-leaf (blue) and bundle-sheath (orange) samples in *Z. mays*. (Supports Figure 3.) CA; *Carbonic Anhydrase*, PEPC; *Phosphoenolpyruvate carboxylase*, PPDK; Pyruvate, *orthophosphate dikinase*, MDH; *Malate dehydrogenase*, NADP-ME; *NADP-dependent malic enzyme*, RBCS1A; *Ribulose bisphosphate carboxylase small subunit1A*, OAA; Oxaloacetate, Mal; Malate, PEP; Phosphoenolpyruvate, Pyr; Pyruvate, Asp; Aspartate.